Journal of Alloys and Compounds 480 (2009) 392–396

Contents lists available at ScienceDirect

Journal of Alloys and Compounds

journal homepage: www.elsevier.com/locate/jallcom

Characterization and formation mechanism of nanocrystalline $(Fe,Ti)_3Al$ intermetallic compound prepared by mechanical alloying

M. Rafiei, M.H. Enayati*, F. Karimzadeh

Department of Materials Engineering, Isfahan University of Technology, Isfahan 84156-83111, Iran

ARTICLE INFO

Article history:
Received 8 January 2009
Received in revised form 14 February 2009
Accepted 17 February 2009
Available online 4 March 2009

Keywords:
Nanostructured materials
Mechanical alloying
Intermetallics

ABSTRACT

The nanocrystalline $(Fe,Ti)_3Al$ intermetallic compound was synthesized by mechanical alloying (MA) of elemental powder with composition $Fe_{50}Al_{25}Ti_{25}$. The structural changes of powder particles during mechanical alloying were studied by X-ray diffractometry and microhardness measurements. Morphology and cross-sectional microstructure of powder particles were characterized by scanning electron microscopy. It was found that a Fe/Al/Ti layered structure was formed at the early stages of milling followed by the formation of Fe(Ti,Al) solid solution. This structure transformed to $(Fe,Ti)_3Al$ intermetallic compound at longer milling times. Upon heat treatment of $(Fe,Ti)_3Al$ phase the degree of DO_3 ordering was increased. The $(Fe,Ti)_3Al$ compound exhibited high microhardness value of about 1050 Hv.

1. Introduction

There is a growing interest in the production of nanocrystalline material because of their excellent physical and mechanical properties compared with coarse-grained materials [1]. Iron aluminides based on Fe_3Al have attracted considerable attention as potential candidates for hot structural application and as promising substitutes for stainless steel and cast iron at room temperature [2–4]. This is because of the availability of raw materials, relatively low density (compared with Fe- and Ni-based alloys), and excellent oxidation and corrosion resistance [5]. However application of iron aluminides is limited because of inherent brittleness of the intermetallic phases. This can be overcome by several ways including refinement of the grain size [6].

A wide variety of methods including casting, powder metallurgy and self-propagation high temperature synthesis (SHS), hydrogen arc plasma and mechanical alloying (MA) are introduced for the synthesis of intermetallic compounds [7,8]. MA process has advantage of direct producing nanocrystalline structure [9–11].

Recently much attention has been given to the investigations of metastable phases in Fe–Al system by MA [7]. Liu et al. [12] reported that a bcc Fe(Al) solid solution, rather than the FeAl intermetallic compound, tended to form for $Fe_{50}Al_{50}$ powder but Enayati and Salehi [7] investigated the formation of Fe_3Al and FeAl intermetallic compounds by MA and reported that no intermediate phase, i.e. solid solution was formed during MA as a precursor to the intermetallic phase. However there are a few reports in the literature on the MA of ternary Fe–Al–Ti powders. Krasnowski and Matyja [13] studied the structural and phase transformation during MA of ternary $Al_{50}Fe_{25}Ti_{25}$ alloy in a high-energy planetary ball mill and reported the formation of amorphous phase. On subsequent heating the τ_2 phase (Al_2FeTi) and the bcc Fe(Al,Ti) solid solution crystallized at about 560 °C. Zhu and Iwasaki [14] investigated the effects of Ti substitution for Fe in Fe_3Al system in the MA process. They reported that mechanical alloying of blended elemental $Fe_xAl_{25}Ti_{75-x}$ (x = 75, 70, 65, 60) powders led to the formation of nanocrystalline Fe(Al,Ti) solid solution with bcc structure. This phase transformed to $(Fe,Ti)_3Al$ intermetallic compound after heating to a temperature range of 350–500 °C. They also reported that the Fe substitution by Ti in Fe_3Al reduced the final powder particle size, shortened the milling time for solid-solution formation, decreased the final crystallite size, increased the lattice parameter of solid solution and enhanced the degree of DO_3 ordering in annealed powders. It has been reported that the addition of Ti to Fe_3Al compound significantly raised the DO_3–B_2 transition temperature and led to the precipitation strengthening at elevated temperatures [15,16]. Zhu et al. [2] have reported that addition of Ti to Fe_3Al can improve its tribological properties. In this work we studied the formation mechanism of $(Fe,Ti)_3Al$ intermetallic compound and microstructure changes during MA process.

2. Experimental methods

Fe, Al and Ti elemental powders with purity of 99.8, 99.5 and 99.7%, respectively, were mixed to give nominal composition of $Fe_{50}Al_{25}Ti_{25}$ (at.%). Fig. 1 shows scanning electron microscopy (SEM) micrographs of elemental Fe, Al and Ti powder particles. As seen the Fe particles had a nearly uniform size of ~100 μm. Al particles were

* Corresponding author. Tel.: +98 311 3915730; fax: +98 311 3912752.
E-mail address: ena78@cc.iut.ac.ir (M.H. Enayati).

0925-8388/$ – see front matter © 2009 Elsevier B.V. All rights reserved.
doi:10.1016/j.jallcom.2009.02.072

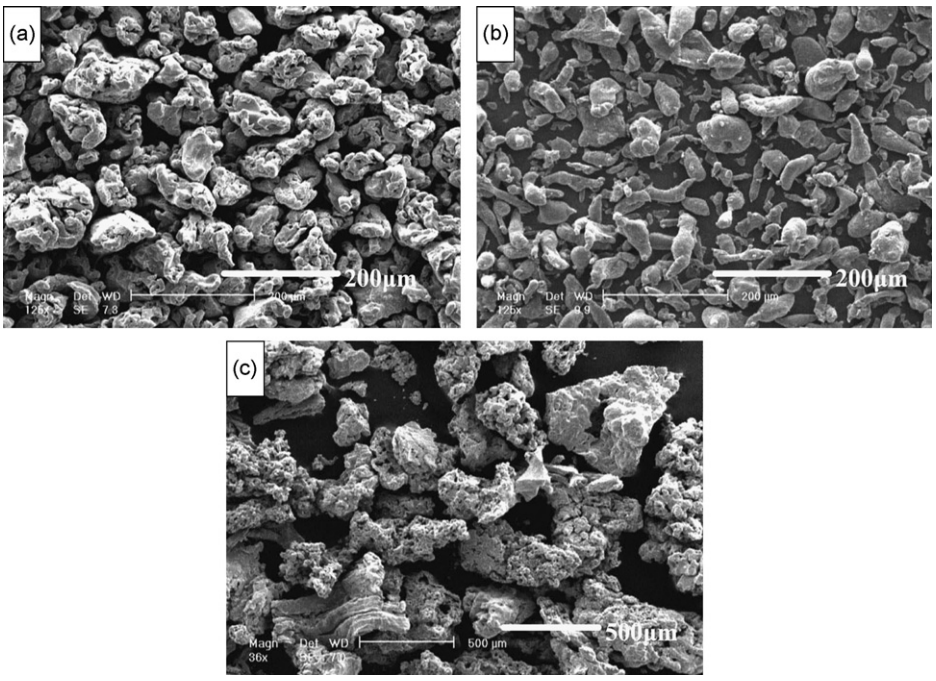

Fig. 1. Secondary electron SEM micrographs of as-received elemental powder particles: (a) Fe, (b) Al and (c) Ti.

irregular in shape with a size distribution of 50–100 μm and Ti particles had a sponge structure with a size distribution of 400–500 μm.

MA was carried out in a high-energy planetary ball mill (home-built), nominally at room temperature under Ar atmosphere. Details of ball mill machine and MA conditions are given in Table 1. No process control agent was added to powder mixture. Samples were taken at selected time intervals and characterized by X-ray diffraction (XRD) in a Philips X' PERT MPD diffractometer using filtered Cu Kα radiation (λ = 0.1542 nm). Morphology and microstructure of powder particles were characterized by SEM in a Philips XL30. The mean powder particle size was estimated from SEM images of powder particles by image tool software. The average size of about 50 particles was calculated and reported as mean powder particle size. Isothermal annealing was carried out to study the thermal behavior of milled powders. MA samples were sealed and then annealed in a conventional furnace. The structural transition occurred during annealing were determined by XRD. The hardness of cross-section of powder particles was also determined by microhardness test using a Vickers indenter at the load of 100 g and dwell time of 5 s. The average of five measurements for each sample was calculated and reported as hardness value.

3. Results and discussion

3.1. Structural evolution

Fig. 2 shows XRD patterns of $Fe_{50}Al_{25}Ti_{25}$ powder mixture as-received and after different milling times. As seen during MA the intensity of Fe, Al and Ti diffraction peaks decreases and their width increase progressively with increasing milling time. Furthermore Fe peaks shift toward lower angles (Fig. 2b) owning to the dissolution of Al and Ti in Fe lattice during milling and concurrent development of Fe(Ti,Al) solid solution with a bcc structure. Increasing milling time to 40 h led to complete disappearance of Al and Ti peaks. These results are in agreement with previous results given by Zhu and Iwasaki [14]. As seen in Fig. 2 traces of $(Fe,Ti)_3Al$ peaks are appeared on XRD pattern after 40 h milling indicating that Fe(Al,Ti) solid solution transformed to $(Fe,Ti)_3Al$ intermetallic compound with DO_3 structure. Continued milling increased the fraction of $(Fe,Ti)_3Al$ intermetallic compound. The direct formation of $(Fe,Ti)_3Al$ phase during milling process has not been reported yet. Although Zhu and Iwasaki reported the formation of this phase upon heating in DTA at temperature range of 350–500 °C [14]. Lack of superlattice diffraction peaks for $(Fe,Ti)_3Al$ phase formed during MA suggests that the crystalline $(Fe,Ti)_3Al$ phase has a disordered structure. The crystallite size and internal strain of $(Fe,Ti)_3Al$ phase were calculated by analyzing XRD peak broadening using the Williamson–Hall method

Table 1
Details of ball mill machine and MA conditions.

Rotation speed of disc (rpm)	250
Rotation speed of vial (rpm)	500
Diameter of disc (mm)	350
Diameter of vial (mm)	90
Vial material	Hardened Cr steel
Capacity of vial (ml)	120
Ball material	Hardened carbon steel
Diameter of balls (mm)	20
Number of balls	5
Balls to powder weight ratio	10:1
Total powder mass (g)	17

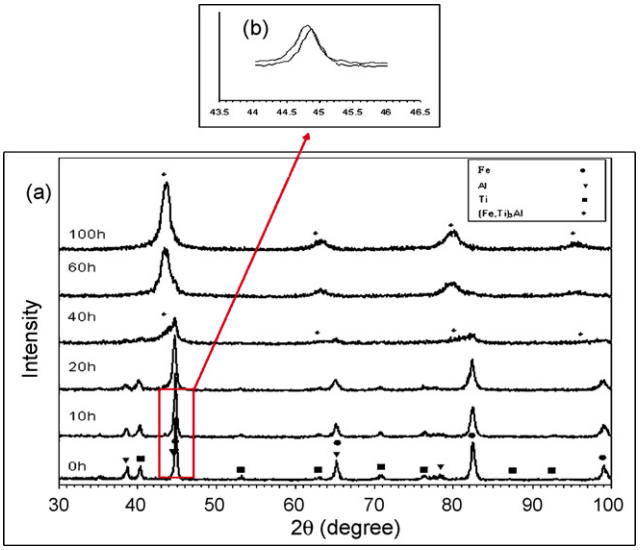

Fig. 2. XRD patterns of $Fe_{50}Al_{25}Ti_{25}$ powder mixture after different milling times. Inset shows the displacement of (1 1 0) Fe peak.

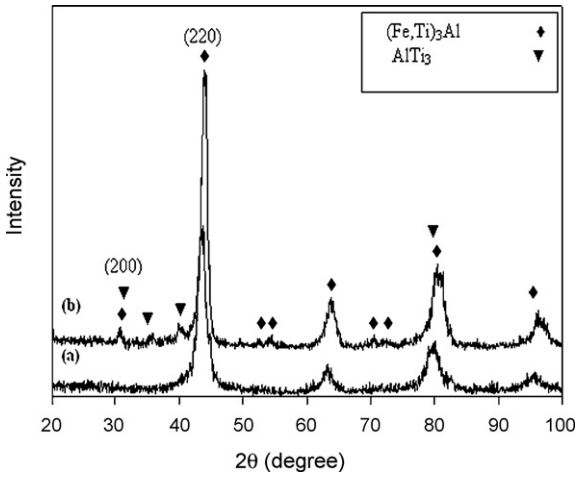

Fig. 3. XRD patterns of powder mixture (a) as-milled for 60 h and (b) after subsequent heat treatment at 550 °C for 1 h.

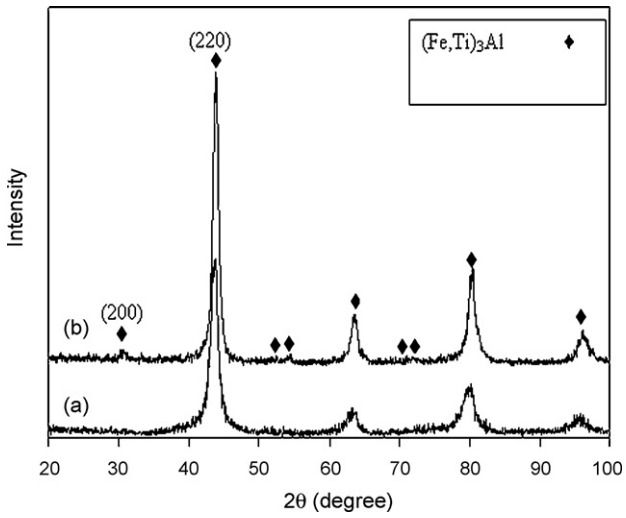

Fig. 4. XRD patterns of powder mixture (a) as-milled for 100 h and (b) after subsequent heat treatment at 550 °C for 1 h.

[17]. The average crystallite size and internal strain were ~12 nm and ~1.5%, respectively. Enayati and Salehi [7] reported that the crystallite size of Fe_3Al phase after 100 h milling was about 14 nm, indicating that the substitution of Ti for Fe in Fe_3Al system has no significant effect on final crystallite size.

Formation of $(Fe,Ti)_3Al$ phase during MA was further confirmed by heat treatment experiments. Figs. 3 and 4 show XRD patterns from $Fe_{50}Al_{25}Ti_{25}$ powders as-milled for 60 and 100 h and also after subsequent annealing at 550 °C for 1 h. For 60-h milled powder traces of $AlTi_3$ peaks appeared on XRD pattern after annealing. This reduces the concentration of Ti in $(Fe,Ti)_3Al$ lattice and as a result the $(Fe,Ti)_3Al$ diffraction peaks shift to higher angles. Furthermore the presence of the superlattice diffraction peaks after heat treatment indicates that an increase in degree of DO_3 ordering occurred during annealing. As shown in Fig. 4 after annealing of 100-h milled powder no new phase formed indicating that the resulting structure after 100 h MA is $(Fe,Ti)_3Al$ intermetallic phase. Similar to 60-h milled sample the superlattice XRD peaks appeared after heat treatment. Enayati and Salehi [7] found no superlattice diffraction peak for $Fe_{75}Al_{25}$ prepared by MA even after heat treatment. This may imply that the addition of Ti to Fe–Al system enhances the ordering of structure upon annealing. This accords with the previous results for the same alloys [14]. It is anticipated that the increase in the degree of DO_3 ordering increases the ductility as the more closely spaced dislocations move more freely in a well-ordered structure [18].

As seen in Table 2 the $I_{(200)}/I_{(220)}$ ratio (the intensity ratio of (2 0 0) superlattice peak to the (2 2 0) fundamental peak) and therefore the degree of DO_3 ordering after annealing for 60-h milled sample is higher than that for 100-h milled sample. This can be due to the lower density of lattice defects in 60-h milled powder. The average crystallite size and internal strain after heat treatment for 100-h milled powder were about 15 nm and 0.86%, respectively.

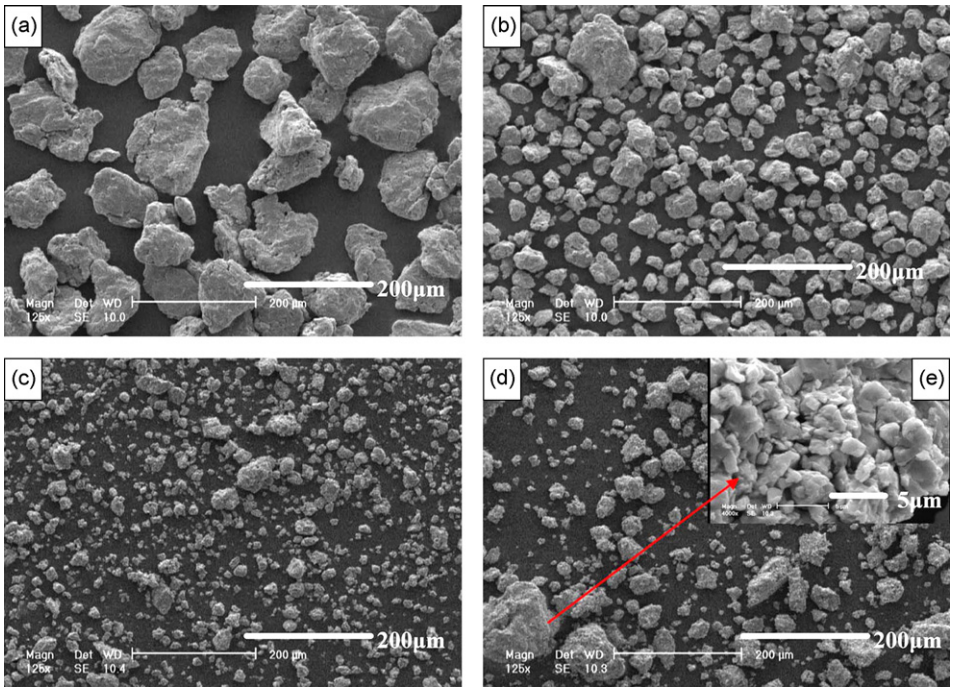

Fig. 5. Secondary electron SEM micrographs of $Fe_{50}Al_{25}Ti_{25}$ powder particles after (a) 5 h, (b) 20 h, (c) 60 h and (d and e) 100 h of milling times.

Table 2
Crystallite size, internal strain, and ordering parameter of powder particles at different conditions.

Condition	Crystallite size (nm)	Internal strain (%)	$I_{(200)}/I_{(220)}$ ratio
60 h MA	20	2	–
60 h MA + annealing	25	1.5	0.088
100 h MA	12	1.5	–
100 h MA + annealing	15	0.86	0.058

As seen annealing has more significant effect on reducing internal strain than crystallite growth.

3.2. Morphological changes

SEM images of powder particles after 5, 20, 60 and 100 h of milling times are shown in Fig. 5. After 5 and 20 h the powder particles were more or less uniform in size and had equiaxed morphology. The mean powder particle size was about 130 ± 15 μm after 5 h which decreased to 45 ± 15 μm after 20 h of milling time. As MA continued for 60 h and then 100 h the powder particle size became more non-uniform. The mean powder particle size after 60 and 100 h of milling times were about 20 ± 10 and 30 ± 8 μm, respectively. Fig. 6 plots the mean powder particle size after different milling times. In early stages of MA the powder particle size decreased sharply due to the predominance of the fracturing of powder particles over the cold welding process. After 60 h of milling time (Fig. 5c) the average particle size reduced to about 20 μm because of formation of brittle $(Fe,Ti)_3Al$ phase. As seen in Fig. 5d the powder particle size after 100 h of milling time appeared to have larger size compared with 60 h milling. Higher magnification of powder particles revealed that the large particles in this stage are in fact an agglomeration of many smaller particles, Fig. 4e.

3.3. Microstructural observations

Cross-sectional SEM images of powder particles after different milling times are shown in Fig. 7. Since back scatter (BS) signals are correlated to the atomic number of elements, bright, grey and dark areas in SEM images correspond to Fe, Ti and Al, respectively. As seen after 2 h of milling time the layered structure is not formed perfectly yet (Fig. 7a). Increasing milling time to 5 h led to the formation of a layered structure (Fig. 7b) consisting of cold welded Fe, Al and Ti layers. At this stage the layers are coarse and non-uniform. Increasing milling time to 10 h (Fig. 7c) led to the refinement of layered structure as a result of repeated cold welding and fracturing. This structure has an extensive Fe/Al/Ti interface. High density of dislocations within layers and extensive interface area [19] promote the Fe–Al–Ti interdiffusion across the layers and therefore the formation of $(Fe,Ti)_3Al$ phase. As a result the layered structure disappeared after 100 h of milling time.

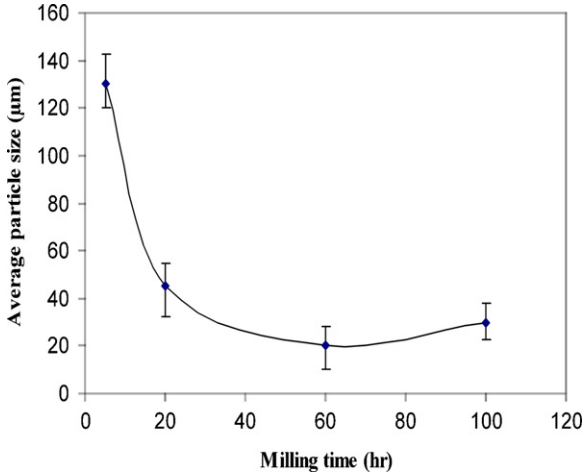

Fig. 6. The average $Fe_{50}Al_{25}Ti_{25}$ powder particle size versus milling time.

3.4. Microhardness measurements

Fig. 8 shows microhardness values of powder particles after different milling times. As can be seen increasing milling time to 10 h led to an increase in hardness value due to the plastic

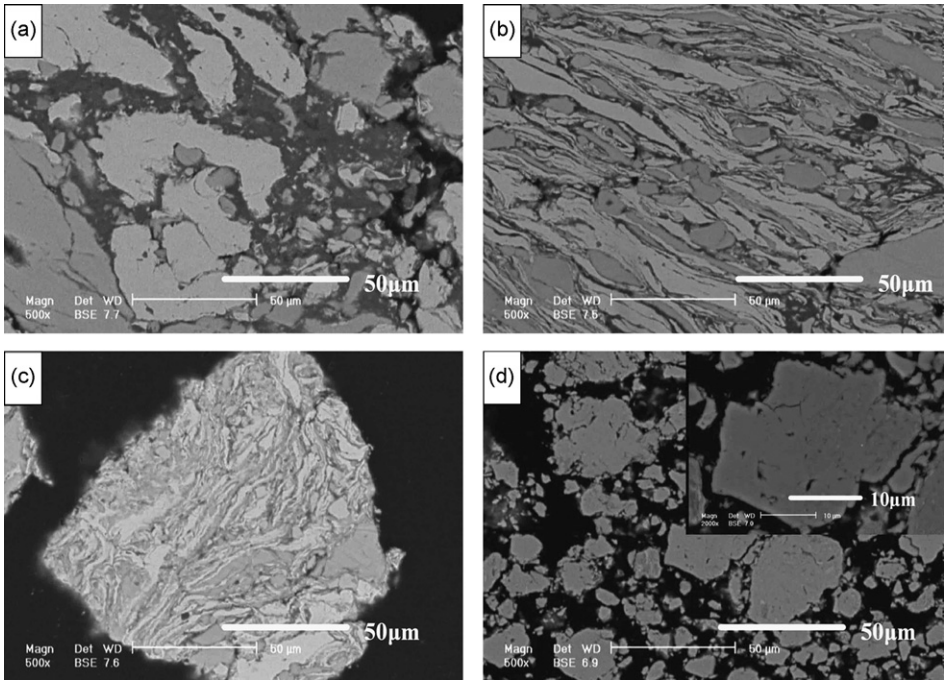

Fig. 7. Cross-sectional back scattered SEM images of powder particles after (a) 2 h, (b) 5 h, (c) 10 h and (d) 100 h of milling times.

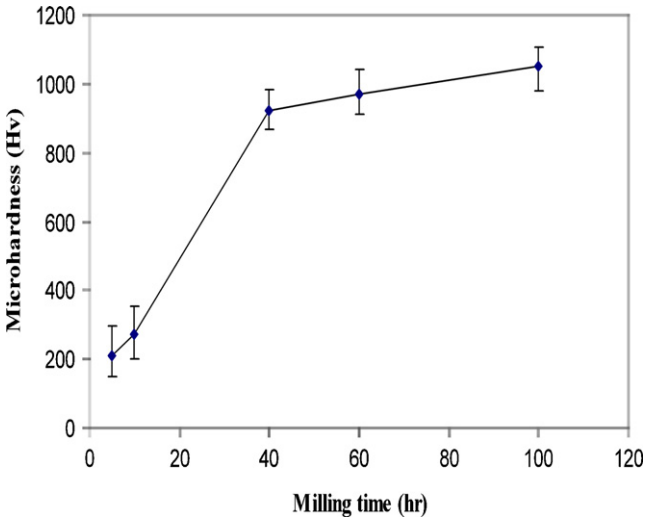

Fig. 8. Microhardness values of cross-section of powder particles as a function of milling time.

deformation induced during MA and therefore consequent work hardening. In addition the solute atoms can increase the hardness by solid-solution hardening mechanism. Zhu et al. [20] investigated the effect of Ti addition on mechanical behavior of Fe_3Al and reported that Ti substitution for Fe increases the lattice parameter and therefore Ti would have a strong solid-solution strengthening effect in Fe_3Al. They also reported Ti-added Fe_3Al alloys exhibited significant strain hardening. By increasing milling time to 40 h a significant increase in hardness value is yielded owning to the formation of $(Fe,Ti)_3Al$ phase in consist with XRD results. Increasing milling time from 40 to 100 h increases the hardness value with a much slower rate mainly due to the increasing volume fraction of $(Fe,Ti)_3Al$ phase. It is worth noting that the hardness value of 1050 Hv obtained after 100 h of milling time is significantly higher than 308 Hv obtained for $(Fe,Ti)_3Al$ wire prepared by arc-melting [20].

4. Conclusions

Nanostructured $(Fe,Ti)_3Al$ intermetallic compound powder was successfully synthesized by mechanical alloying of $Fe_{50}A_{25}Ti_{25}$ powder mixture. In early stages of milling a Fe/Al/Ti layered structure was formed, which progressively refined with increasing milling time. This structure transformed to a Fe(Al,Ti) solid solution and then $(Fe,Ti)_3Al$ intermetallic DO_3 phase on further milling. Annealing of milled powder led to the ordering of DO_3 structure. It was found that the addition of Ti to Fe–Al system enhanced the ordering of structure upon annealing but has no significant effect on final crystallite size. $(Fe,Ti)_3Al$ phase exhibited a high microhardness value of about 1050 Hv.

References

[1] S. Eghtesadi, N. Parvin, M. Rezaee, M. Salari, J. Alloys Compd. 473 (2009) 557–559.
[2] S.M. Zhu, M. Tamura, K. Sakamoto, K. Iwasaki, Mater. Sci. Eng. A 292 (2000) 83–89.
[3] N.S. Stoloff, Mater. Sci. Eng. A 258 (1998) 1–14.
[4] C.T. Liu, E.P. George, P.L. Maziasz, J.H. Schneffiel, Mater. Sci. Eng. A 258 (1998) 84–98.
[5] K. Matsuura, Y. Obara, M. Kudoh, ISIJ Int. 46 (2006) 871–874.
[6] A.V. Leonov, V.I. Fadeeva, O.E. Gladilina, H. Matyja, J. Alloys Compd. 281 (1998) 275–279.
[7] M.H. Enayati, M. Salehi, J. Mater. Sci. 40 (2005) 3933–3938.
[8] H. Chuncheng, C. Zuolin, Y. Yansheng, Z. Zhikun, J. Nanopart. Res. 4 (2002) 107–110.
[9] B.G. Park, S.H. Ko, Y.H. Park, J.H. Lee, Intermetallics 14 (2006) 660–665.
[10] M.H. Enayati, F. Karimzadeh, S.Z. Anvari, J. Mater. Proc. Technol. 200 (2008) 312–315.
[11] H.G. Tang, X.F. Ma, W. Zhao, X.W. Yan, R.J. Hong, J. Alloys Compd. 347 (2002) 228–230.
[12] Z.G. Liu, J.T. Guo, L.L. He, Z.Q. Hu, Nanostruct. Mater. 4 (1994) 787–794.
[13] M. Krasnowski, H. Matyja, J. Alloys Compd. 319 (2001) 296–302.
[14] S.M. Zhu, K. Iwasaki, Mater. Sci. Eng. A 270 (1999) 170–177.
[15] R.T. Fortnum, D.E. Mikkola, Mater. Sci. Eng. 91 (1987) 223–231.
[16] M.G. Mendiratta, S.K. Ehlers, H.A. Lipsitt, Metall. Trans. A 18 (1987) 509–518.
[17] G.K. Williamson, W.H. Hall, Acta Metall. 1 (1953) 22–31.
[18] J.M. Cairney, P.R. Munroe, J. Mater. Sci. Lett. 18 (1999) 449–452.
[19] M.H. Enayati, D.Phil. Thesis, University of Oxford, 1998.
[20] S.M. Zhu, K. Sakamoto, M. Tamura, K. Iwasaki, Mater. Trans. 42 (2001) 484–490.